

# A dynamical perspective on additional planets in 55 Cancri

Sean N. Raymond<sup>1,2</sup>, Rory Barnes<sup>3</sup> & Noel Gorelick<sup>4</sup>

## ABSTRACT

Five planets are known to orbit the star 55 Cancri. The recently-discovered planet  $f$  at 0.78 AU (Fischer *et al.* 2008) is located at the inner edge of a previously-identified stable zone that separates the three close-in planets from planet  $d$  at 5.9 AU. Here we map the stability of the orbital space between planets  $f$  and  $d$  using a suite of n-body integrations that include an additional, yet-to-be-discovered planet  $g$  with a radial velocity amplitude of  $5 m s^{-1}$  (planet mass = 0.5-1.2 Saturn masses). We find a large stable zone extending from 0.9 to 3.8 AU at eccentricities below 0.4. For each system we quantify the probability of detecting planets  $b - f$  on their current orbits given perturbations from hypothetical planet  $g$ , in order to further constrain the mass and orbit of an additional planet. We find that large perturbations are associated with specific mean motion resonances (MMRs) with planets  $f$  and  $d$ . We show that two MMRs, 3f:1g (the 1:3 MMR between planets  $g$  and  $f$ ) and 4g:1d cannot contain a planet  $g$ . The 2f:1g MMR is unlikely to contain a planet more massive than  $\sim 20 M_{\oplus}$ . The 3g:1d and 5g:2d MMRs could contain a resonant planet but the resonant location is strongly confined. The 3f:2g, 2g:1d and 3g:2d MMRs exert a stabilizing influence and could contain a resonant planet. Furthermore, we show that the stable zone may in fact contain 2-3 additional planets, if they are  $\sim 50 M_{\oplus}$  each. Finally, we show that any planets exterior to planet  $d$  must reside beyond 10 AU.

*Subject headings:* stars: planetary systems — methods: n-body simulations — methods: statistical

---

<sup>1</sup>Center for Astrophysics and Space Astronomy, University of Colorado, UCB 389, Boulder CO 80309-0389; raymond@lasp.colorado.edu

<sup>2</sup>NASA Postdoctoral Program Fellow.

<sup>3</sup>Lunar and Planetary Laboratory, University of Arizona, Tucson, AZ

<sup>4</sup>Google, Inc., 1600 Amphitheatre Parkway, Mountain View, CA 94043

## 1. Introduction

In a remarkable study, Fischer *et al.* (2008) have measured the orbits of five planets orbiting the star 55 Cancri, the most planets of any exoplanet system to date. The system contains two strongly-interacting, near-resonant giant planets at 0.115 and 0.24 AU (Butler *et al.* 1997; Marcy *et al.* 2002), a ‘hot Neptune’ at 0.038 AU (McArthur *et al.* 2004), a Jupiter analog at 5.9 AU (Marcy *et al.* 2002) and a newly-discovered sub-Saturn-mass planet at 0.78 AU (Fischer *et al.* 2008). Table 1 lists Fischer *et al.*’s self-consistent dynamical fit of the orbits of the five known planets in 55 Cancri.

The fast-paced nature of exoplanet discoveries can lead to interesting interactions between theory and observation. Prior to the discovery of planet 55 Cancri *f*, several groups had mapped out the region between planets *c* and *d* to determine the most likely location of additional planets. Most studies used massless test particles to probe the stable zone (Barnes & Raymond 2004 – hereafter BR04; Jones, Underwood & Sleep 2005; Rivera & Haghighipour 2007). Test particles are good proxies for small, Earth-sized planets because they simply react to the ambient gravitational field. However, they are not good substitutes for fully-interacting, real planets. Thus, Raymond & Barnes (2005; hereafter RB05) mapped out this zone using Saturn-mass test planets. The stable zone from BR04 and RB05 extended from 0.7 AU to 3.2-3.4 AU, a region that includes the star’s habitable zone (Raymond, Barnes & Kaib 2006). The planet 55 Cnc *f* was discovered by Fischer *et al.* at the inner edge of that stable zone.

The “Packed Planetary Systems” (PPS) hypothesis asserts that if a zone exists in which massive planets are dynamically stable, then that zone is likely to contain a massive planet (BR04, RB05, Raymond *et al.* 2006; Barnes, Godziewski & Raymond 2008). Although the idea behind the PPS hypothesis is not new (see, for instance, Laskar 1996), the large number of planetary systems being discovered around other stars allows PPS to be tested directly. Indeed, the  $\sim 1.4$  Saturn mass planet HD 74156 *d* recently discovered by Bean *et al.* (2008) was located in the stable zone mapped out in BR04 and RB05, and with the approximate mass predicted by RB05 (Barnes *et al.* 2008). In addition, most of the first-discovered planetary systems are now known to be packed (Barnes *et al.* 2008), as well as  $\sim 85\%$  of the known two-planet systems (Barnes & Greenberg 2007). The fact that 55 Cancri *f* lies within the stable zone identified in previous work (BR04; RB05) also supports PPS, especially since planets *e* through *c* are packed, i.e. no additional planets could exist between them. Several other planet predictions have been made and remain to be confirmed or refuted (see Barnes *et al.* 2008) – the most concrete outstanding prediction is for the system HD 38529 (see RB05).

Mean motion resonances (MMRs) are of great interest because they constrain theories

of planet formation. Models of convergent migration in gaseous protoplanetary disks predict that planets should almost always be found in low-order MMRs and with low-amplitude resonant libration (Snellgrove *et al.* 2001; Lee & Peale 2002). This may even have been the case for the giant planets in our Solar System (Morbidelli *et al.* 2007). On the other hand, planet-planet scattering can produce pairs of resonant planets in  $\sim 5\%$  of unstable systems, but with large-amplitude libration and often in higher-order MMRs (Raymond *et al.* 2008). Thus, understanding the frequency and character of MMRs in planetary systems is central to planet formation theory.

In the context of PPS, 55 Cancri is an important system as it contains many planets, but still appears to have a gap large enough to support more planets. Therefore, PPS makes a clear prediction that another planet must exist between known planets  $f$  and  $d$ . In this paper we add massive hypothetical planets to the system identified by Fischer *et al.* (2008) to determine which physical and orbital properties could still permit a stable planetary system. We focus our search on the “new” stable zone between planets  $f$  and  $d$ . We also show that certain dynamically stable configurations are unlikely to contain a planet because the large eccentricity oscillations induced in the known planets significantly reduce the probability of Fischer *et al.* having detected the known planets on their identified orbits, to within the observational errors. The orbital regions that perturb the known planets most strongly correlate with specific dynamical resonances, such that we can put meaningful constraints on the masses of planets in those resonances. Finally, we also use test particle simulations to map out the region of stability for additional planets beyond planet  $d$ , in the distant reaches of the planetary system.

## 2. Methods

Our analysis consists of four parts; the methods used for each are described in this section. First, we map the stable zone between planets  $f$  and  $d$  using massive test planets – note that we use the term “test planets” to refer to massive, fully-interacting planets. Our numerical methods are described in § 2.1.1. Second, we use massless test particles to map the stability of orbits exterior to planet  $d$ , as described in § 2.1.2. Third, we use the same technique to map several mean motion resonances in the stable region. A simple overview of resonant theory is presented in §2.2. Finally, we use a quantity called the FTD – defined in § 2.3 – to evaluate the probability of detecting stable test planets.

## 2.1. Numerical Methods

### 2.1.1. Massive test planets

We performed 2622 6-planet integrations of the 55 Cancri planetary system which include an additional hypothetical planet  $g$  located between known planets  $f$  and  $d$ . In each case, the known planets began on orbits from Table 1 including randomly-assigned mutual inclinations of less than 1 degree. Planet  $g$  was placed from 0.85 to 5.0 AU in increments of 0.03 AU and with eccentricity between 0.0 and 0.6 in increments of 0.033. The mass of planet  $g$  was chosen to induce a reflex velocity of  $5 \text{ m s}^{-1}$  in the  $0.92 M_{\odot}$  host star (Valenti & Fischer 2005): its mass was varied continuously from  $\sim 50 M_{\oplus}$  inside 1 AU to  $120 M_{\oplus}$  at 5 AU. Orbital angles of the planets  $g$  were chosen at random. The system was integrated for 10 Myr using the symplectic integrator `Mercury` (Chambers 1999), based on the Wisdom-Holman mapping (Wisdom & Holman 1991) We used a 0.1 day timestep and all simulations conserved energy to better than 1 part in  $10^6$ . Integrations were stopped when they either reached 10 Myr or if a close encounter occurred between any two planets such that their Hill radii overlapped.

Although 10 Myr is much less than the typical ages of extrasolar planetary systems ( $\sim \text{Gyr}$ ), for a survey of this magnitude it is impractical to simulate each case for Gyrs. Previous N-body integrations of extrasolar planets have shown that  $10^6$  orbits is sufficient to identify  $\sim 99\%$  of unstable configurations (Barnes & Quinn 2004). Moreover, N-body models of stability boundaries are consistent with alternative methods, such as the Mean Exponential Growth of Nearby Orbits (MEGNO; Cincotta & Simo 2000) or Fast Lyapunov Indicators (Froslché *et al.* 1998; Sándor *et al.* 2007). For example, 1 Myr N-body integrations of the 2:1 resonant pair in HD 82943 (Barnes & Quinn 2004) identified a stability boundary that is very close to that of a MEGNO calculation (Goździewski & Maciejewski 2001). More recently, Barnes & Greenberg (2006a), using 1 Myr N-body integrations, derived a quantitative relationship between the Hill and Lagrange stability boundaries for the non-resonant planets in HD 12661 that is nearly identical to a MEGNO study (Šidlichovský & Gerlach 2008). Therefore, for both resonant and non-resonant cases,  $10^7$  year integrations provide a realistic measurement of stability boundaries.

In Section 4, we performed several thousand additional integrations but with hypothetical planet  $g$  in or near specific mean motion resonances (MMRs) with planet  $f$  or  $d$ . In each case we aligned planet  $g$ 's longitude of pericenter  $\varpi$  and time of perihelion with either planet  $f$  or  $d$  unless otherwise noted. Small mutual inclinations ( $< 1 \text{ deg}$ ) between the two planets were included, with random nodal angles. Each set of simulations focused on a given MMR and included test planets of fixed mass with a range of orbital parameters designed to cover

the MMR. The number of simulations ranged from 30 (4g:1d) to >1100 (2g:1d) simulations per set. Planet  $g$ 's mass was constant in each set of simulations but varied by a factor of 2-3 between sets from the maximum value ( $RV = 5 \text{ m s}^{-1}$ ) down to 10-40  $M_{\oplus}$ . We performed 2-3 sets for each MMR.

Our results are clearly sensitive to the assumed “true” orbits and masses of planets  $b - f$ . For this work we have adopted Fischer *et al.*'s (2008) self-consistent dynamical fit, but the observational uncertainties remain large. However, the locations of the MMRs in question scale simply with the semimajor axis of planet  $d$  or  $f$ . The strength of these MMRs depends on the mass and eccentricity of planets  $d$  or  $f$  (e.g., Murray & Dermott 1999). The eccentricity of planet  $d$  is relatively well-known, while that of planet  $f$  is weakly constrained. Thus, the system parameters that could affect our results are  $e_f$ ,  $M_d$  and  $M_f$ . Since we assumed a small value of  $e_f$ , any increase would affect the strength of the 3f:2g, 2f:1g, and 3f:1g MMRs. If  $M_f$  and  $M_d$  increase due to a determination of the system's observed inclination, then all the resonances we studied will increase in strength. This will tend to destabilize planets and also increase the size of chaotic zones. Thus, our results are likely to be “lower limits” in terms of the strength of resonances. Despite these potential issues, our simulations provide a realistic picture of the (in)stability of each MMR.

### 2.1.2. Massless Test Particles

To give a more complete view of the planetary system, we also tested the stability of planets exterior to planet  $d$  (5.9 AU). We used massless test particles for these simulations because of their smaller computational expense. Test particles were spaced by 0.01 AU from 6 to 30 AU (2401 total particles), and were given zero eccentricity, zero inclination orbits. All five known planets were included with orbits from Table 1, including randomly assigned inclinations of less than 1 degree. As in previous runs, we used the `Mercury` hybrid integrator (Chambers 1999) with a 0.1 day timestep and integrated the system for 10 Myr.

## 2.2. Theory of Mean Motion Resonances (MMRs)

For mean motion resonance  $p+q : p$ , the resonant arguments  $\theta_i$  (also called “resonant angles”) are of the form

$$\theta_{1,2} = (p + q)\lambda_1 - p\lambda_2 - q\varpi_{1,2} \quad (1)$$

where  $\lambda$  are mean longitudes,  $\varpi$  are longitudes of pericenter, and subscripts 1 and 2 refer to the inner and outer planet, respectively (e.g., Murray & Dermott 1999). Resonant arguments

effectively measure the angle between the two planets at the conjunction point – if any argument librates rather than circulates, then the planets are in mean motion resonance. In fact, the bulk of resonant configurations are characterized by only one librating resonant argument (Michtchenko *et al.* 2008). In general, libration occurs around equilibrium angles of zero or  $180^\circ$  but any angle can serve as the equilibrium. Different resonances have different quantities of resonant arguments, involving various permutations of the final terms in Eq. 1. For example, the 2:1 MMR ( $q=1, p=1$ ) has two resonant arguments, and the 3:1 MMR ( $q=2, p=1$ ) has three arguments:

$$\theta_1 = 3\lambda_1 - \lambda_2 - 2\varpi_1, \quad \theta_2 = 3\lambda_1 - \lambda_2 - 2\varpi_2, \quad \text{and} \quad \theta_3 = 3\lambda_1 - \lambda_2 - (\varpi_1 + \varpi_2). \quad (2)$$

In Section 4, we focus on the possibility of a hypothetical planet  $g$  existing in several MMRs in the stable zone between planets  $f$  and  $d$ . We measure the behavior of planets in and near resonance using the appropriate resonant arguments, as well as the relative apsidal orientation, i.e.,  $\varpi_g - \varpi_{d,f}$ .

### 2.3. The FTD value (“Fraction of Time on Detected orbits”)

We have developed a simple quantity to constrain the location of hypothetical planet  $g$  beyond a simple stability criterion. To do this, we consider the observational constraints on the orbits of known planets  $b - f$  (1-sigma error bars from Fischer *et al.* (2008) are listed in Table 1). A stable test planet can induce large oscillations in the eccentricities of the observed planets. Systems undergoing large eccentricity oscillations can be stable indefinitely as long as their orbits remain sufficiently separated (Marchal & Bozis 1982; Gladman 1993; Barnes & Greenberg 2006a, 2007). However, systems with large eccentricity oscillations are less likely to be observed in a specific eccentricity range, especially with all planets having relatively small eccentricities, as is the case for 55 Cancri. The probability that a hypothetical planet  $g$  can exist on a given orbit is related to the fraction of time that known planets  $b - f$  are on their current orbits, to within the observational error bars. We call this quantity the FTD (“Fraction of Time on Detected orbits”). If the FTD is small, then it is unlikely for planet  $g$  to exist on that orbit, because perturbations from planet  $g$  have decreased the probability of the *already-made*-detection of planets  $b - f$ . However, if the FTD is close to 1 then planet  $g$  does not significantly affect the likelihood of detecting the other planets and therefore hypothetical planet could exist on the given orbit. We have calibrated the FTD to have a value of unity for the known five-planet system (with no planet  $g$ ). To perform this calibration, we artificially increased the observational error of planet  $c$  from 0.008 to 0.013. This was necessary simply because the evolution of the five known planets causes planet  $c$ ’s

eccentricity to oscillate with an amplitude that is larger than its observational uncertainty, such that the FTD of the 5-planet system is  $\sim 0.65$ . Thus, we calibrate by artificially increasing the uncertainty to roughly match the oscillation amplitude. As the region of interest lies between planets  $f$  and  $d$ , low FTD values are virtually always due to increases in the eccentricities of planets  $f$  or  $d$ . The small change we made to the error of planet  $c$  does not affect our results, and different methods for calibrating the FTD yield similar values. The FTD value therefore represents a quantity that measures the perturbations of a hypothetical planet  $g$  on the detectability of observed planets  $b - f$ , normalized to the amplitude of the self-induced perturbations of planets  $b - f$ .

To summarize, regions of high FTD (white in upcoming figures) represent orbits of planet  $g$  which are consistent with current observations of the system. Regions of low FTD (blue or black) represent orbits which significantly decrease the probability of detecting planets  $b - f$  on their observed orbits. Thus, we do not expect an additional planet to exist in regions with low FTD. Our confidence in this assertion scales with the FTD value itself (see color bar in upcoming figures). We a low FTD value to be below 50%, although this choice is arbitrary and much of the dynamical structure of the stable region is revealed at FTD values above 0.5. Note that all regions that have an FTD value are dynamically stable for our 10 Myr integration.

### 3. The stable zone between planets $f$ and $d$

Figure 1 shows the stable zone between planets  $f$  and  $d$ : 984 of the 2622 simulations were stable (37.5%). Hatched areas indicate unstable regions, white and grey/blue indicate stable zones. The inner edge of the stable zone is defined by orbits that approach within a critical distance of planet  $f$  (the dashed line denotes orbits that cross those of planets  $f$  or  $d$ ). The outer regions of the stable zone are carved by resonances with the  $\sim 4$  Jupiter-mass planet  $d$ . Virtually no stable regions exist exterior to the 2:1 mean motion resonance (MMR) with planet  $d$  at 3.7 AU, except for the 3:2 MMR at  $\sim 4.5$  AU (not all test planets at 4.5 AU in Fig 1 are in resonance because angles were chosen randomly). Note that the outer boundary of the stable zone is more distant than the one mapped in RB04 and BR05 – this is due to a decrease in the best-fit eccentricity of planet  $d$ , reducing the strength of its secular and resonant perturbations. For a given semimajor axis and eccentricity of test planet  $g$ , the bluescale of Fig 1 represents the FTD, i.e. the probability of detecting known planets  $b - f$  on their current orbits (see color bar). The dark observationally unlikely areas do not fall at random, but are associated with specific dynamical structures within the stable zone. The wide, dark band from 1.3-2 AU with  $e \sim 0.2 - 0.4$  are orbits for which secular perturbations

from planet  $g$  increase the eccentricity of planet  $f$  above 0.2. The wide dark dip from 2-2.4 AU at smaller eccentricities is associated with a secular resonance between planets  $f$  and  $g$  which also increases the eccentricity of planet  $f$  above its observational limit. All other observationally unlikely (i.e., low FTD, dark) regions are caused by MMRs with planets  $f$  or  $d$ , although some are not clearly resolved in Fig. 1 because the resonance is narrow. There is clearly room in between planets  $f$  and  $c$  for an additional planet; in § 5 we explore the possibility that multiple companions might lie in this zone.

#### 4. Mean motion resonances (MMRs)

We performed extensive additional simulations to test the stability of parameter space in the vicinity of eight resonances in the stable zone – 2g:3f (the 2:3 MMR between planets  $g$  and  $f$ ), 1g:2f, 1g:3f, 4g:1d, 3g:1d, 5g:2d, 2g:1d and 3g:2d. The location of these resonances is shown in Fig. 1 and listed in Table 2. Based on our results, we divide the eight MMRs into three categories: stable, unstable, and neutral resonances. A stable MMR effectively stabilizes a given region against secular perturbations (i.e., long-term gravitational perturbations far from resonance; see e.g. Murray & Dermott 1999). For example, as seen in Fig. 1, there are locations associated with the 3g:2d MMR at  $\sim 4.5$  AU that, although they cross planet  $d$ 's orbit, are stable for long timescales. Conversely, an unstable resonance destabilizes a region that would be stable under just secular perturbations. For example, the region at 2.8-3.0 AU is well-shielded from secular perturbations, but the 3g:1d MMR at 2.88 AU causes a large swath of nearby orbits to be unstable. A neutral resonance is one where a region would be stable under secular perturbations, and remains stable with the resonance. Although the stability of test planets is not strongly affected by these MMRs, FTD values can be strongly affected, which in turn affect the likelihood of detecting a planet in a neutral resonance.

We see general similarities between different resonances. In many cases there exists a small region that can undergo resonant libration – that region is usually confined in  $a_g$ ,  $e_g$ , and  $M_g$  (the mass of planet  $g$ ) space. Planets in this region undergo regular eccentricity oscillations such that their FTD values are usually quite high, i.e. a planet can exist in that zone. Just outside a resonant region there often exists a chaotic zone in which planets may undergo temporary capture into the resonance. These zones are characterized by large irregular eccentricity variations that can eventually lead to close encounters and dynamical instability. The instability timescale is shorter for smaller  $M_g$  such that these chaotic zones are more populated for large  $M_g$ . However, given the relatively short 10 Myr duration of our integrations, we suspect that these chaotic zones would be cleared out in the system lifetime. We also found that stable zones with apsidal libration often exist close to the resonance.

## 4.1. Stable Resonances – 3f:2g, 2g:1d, and 3g:2d

### 4.1.1. The 3f:2g MMR

The 3f:2g MMR is located from 1.02-1.04 AU. Figure 2 shows the outcome of 136 simulations with planet  $g$  in the resonant region, formatted as in Fig. 1. Two stable peaks extend above the collision line with planet  $f$ , at 1.024 and 1.034-1.039 AU. To avoid a close encounter and maintain dynamical stability, these planets must be in the 3:2 MMR. Indeed, the resonance provides a protection mechanism to maintain stability despite crossing orbits. The resonant dynamics prevents close encounters from happening by phasing orbital angles in various ways (see section 3 of Marzari *et al.* 2006) – this is also the case for the 2g:1d and 3gL2d MMRs. As expected, we find that all planets on the two peaks above the collision line undergo resonant libration of  $\theta_1 = 3\lambda_g - 2\lambda_f - \varpi_g$  about  $180^\circ$ . In the peak at 1.034 AU, resonant orbits extend down to zero eccentricity. However, the resonance associated with the peak at 1.024 AU extends down to  $e_g \sim 0.05$ . Below that limit and for the rest of the nearby, low-eccentricity stable zone, test planets are not in resonance with planet  $f$ .

Figure 3 shows the evolution of a simulation above the collision line with planet  $f$ . Libration of  $\theta_1$  about  $180^\circ$  is apparent. In contrast,  $\varpi_g - \varpi_f$  and  $\theta_2$  are preferentially found near  $0^\circ$  but they do occasionally circulate. If all three angles were librating then the system would be in apsidal corotation resonance; Michtchenko & Beauge 2003; Ferraz-Mello, Michtchenko & Beauge 2003). The eccentricities of planets  $g$  and  $f$  oscillate out of phase with amplitudes of  $\sim 0.3$ . Note that  $e_f$  therefore exceeds the limits of its observational uncertainty, since its nominal current value is  $\sim 0$  with an uncertainty of 0.2. Thus, this simulation has a low FTD value of 0.335.

FTD values for test planets above the collision line are smaller for larger values of  $M_g$ . However, more than half of resonant configurations have very high FTD values. Therefore, a planet as massive as  $54 M_\oplus$  could reside in the 3f:2g MMR, but only at low eccentricity ( $e_g \lesssim 0.2$ ).

### 4.1.2. The 2g:1d MMR

The 2:1 MMR with planet  $d$  (2g:1d) is a wide, stable resonance located from 3.6-3.85 AU, and in some cases extending above the collision line with planet  $d$ . Figure 4 shows the outcomes of our integrations near the resonance. There is a peak of stability from 3.6-3.9 AU, and a sharp cliff of instability for  $a_g > 3.9$  AU. The height of the peak depends on  $M_g$ : the stable region extends to higher  $e$  for more massive planets. The majority of the

stable region in Fig. 4 participates in the 2g:1d MMR, i.e. at least one resonant argument librates. However, the behavior of different resonant arguments varies with  $M_g$ . Figure 5 shows the stable zone from Fig. 4 color-coded by which angle is librating ( $\theta_1 = 2\lambda_d - \lambda_g \varpi_g$  and  $\theta_2 = 2\lambda_d - \lambda_g - \varpi_d$ ). The libration of  $\theta_1$  is widespread and covers a large area. In contrast,  $\theta_2$  librates only in cases with  $M_g = 100 M_\oplus$ , at the center of the resonance, right on the collision line with planet  $d$ . In cases where  $\theta_2$  librates,  $\theta_1$  and  $\varpi_g - \varpi_d$  also librate in a configuration known as an apsidal corotation resonance. For lower  $M_g$ , the apsidal corotation resonance is apparent only in a few cases for  $M_g = 50 M_\oplus$ . It is interesting that the small island of  $\theta_2$  libration for  $M_g = 100 M_\oplus$  has very high FTD values, while surrounding areas, while still in the resonance, have far lower FTD values (Fig. 4). These high FTD areas are shifted to slightly higher  $e_g$  for  $M_g = 50 M_\oplus$  and are in fact unstable for  $M_g = 20 M_\oplus$ . If a planet  $g$  exists in the 2g:1d MMR, then it must be localized in both mass and orbital parameter space. For large  $M_g$ , the planet could be either right on the collision line with planet  $d$  at  $a_g \sim 3.73$  AU and  $e_g \sim 0.5$ , or in the surrounding region of high FTD that extends from 2.6-2.85 AU with  $e_g$  from 0.1-0.4. The lower-FTD belt that separates these two regions has FTD  $\sim 0.7$ , so we cannot firmly exclude planets from that region. For smaller  $M_g$ , only the second region is available, although it reaches slightly higher  $e_g$ .

#### 4.1.3. The 3g:2d MMR

The 3g:2d MMR is the most dramatic example of a stabilizing resonance. The entire resonant region is unstable to secular perturbations (See Fig. 1). Nonetheless, Figure 6 shows that there does exist a contiguous stable region here. Moreover, more than half of the resonant region has orbits that cross that of planet  $d$ . We find that all orbits across the collision line with planet  $d$  exhibit regular libration of the resonant angle  $\theta_1 = 3\lambda_d - 2\lambda_g - \varpi_g$  about  $0^\circ$ , although none undergo apsidal libration. For the majority of cases below the collision line there is a preferential alignment of  $\theta_1$ ,  $\theta_2$ , and  $\varpi_g - \varpi_d$ , but circulation does occur. The situation is similar for the three different values of  $M_g$ , although a larger fraction of systems exhibited stable resonant libration for lower  $M_g$ .

FTD values above the collision line are 0.5-0.8 for  $M_g = 113 M_\oplus$ , 0.8-1 for  $M_g = 50 M_\oplus$ , and 1 for  $M_g = 20 M_\oplus$ . This suggests that the 3g:2d MMR is unlikely to contain a planet more massive than  $\sim 50 M_\oplus$  above the collision line. However, just below the collision line FTD values are large for all masses so we cannot constrain  $M_g$  beyond the stability boundaries.

It is interesting that low-eccentricity test planets are unstable in this region. This appears to be due to short-term dynamical forcing from planet  $d$ , as the low- $e_g$  region does

not participate in the 3g:2d MMR. Planet  $d$ 's Hill sphere is very large,  $\sim 0.65$  AU, such that any body exterior to 4.88 AU will cross planet  $d$ 's orbit unless a favorable alignment (i.e., a resonance) prevents this. For a test planet starting at 4.5 AU, an eccentricity greater than 0.07 will bring the planet into the orbit-crossing region. Secular forcing from planet  $d$  is very strong in the region of the 3g:2d MMR, so any planet not participating in the resonance will be quickly destabilized. For low- $e_g$  orbits near, but not in, the 3g:2d MMR, encounters between planets  $g$  and  $d$  can occur in less than two orbital periods of planet  $d$ .

## 4.2. Unstable Resonances – 3g:1d and 4g:1d

### 4.2.1. The 3g:1d MMR

The 3g:1d MMR is not truly an unstable resonance, although Figure 7 shows that a large region of parameter space centered on the resonance (at  $\sim 2.88$  AU)<sup>1</sup> is destabilized. However, a small range of test planets does show evidence of long-term stable libration of one of the three resonant arguments for the 3:1 MMR (see Eq. 2). This region is located at  $a_g = 2.86$ -2.89 AU and  $e_g \leq 0.06$  (i.e.,  $e_g < e_d$ ). In these cases only one argument,  $\theta_3$ , librates, whereas  $\theta_1$ ,  $\theta_2$ , and  $\varpi_g - \varpi_d$  all circulate. The eccentricities of planets  $g$  and  $d$  oscillate regularly within narrow ranges such that the FTD value of these resonant cases is low. In other words, a configuration with planet  $g$  in 3:1 resonance with planet  $d$  is observationally allowed, although the resonant region is narrow and restricted to very low eccentricities.

Figure 8 shows the evolution of two simulations, one in stable resonant libration and the other undergoing chaotic evolution including a time spent in resonance. In the stable case, the apses of planets  $d$  and  $g$  are circulating but  $\theta_3$  librates consistently with an amplitude of  $60^\circ$ . In contrast, the chaotic (and ultimately unstable) case undergoes resonant libration of  $\theta_1$  for 1.5 Myr, during which  $e_g$  remained confined in a relatively narrow band and  $\varpi_g - \varpi_d$  librated about anti-alignment (see below). Once the resonance was broken,  $e_g$  ranged from close to zero to above 0.5. At 3.2 Myr, planets  $g$  and  $d$  underwent a close encounter and the integration was stopped.

There exists a small “island” near the resonance at  $a_g = 2.85$ -2.88 AU with  $e_g = 0.15$ –0.2 which is stable for long timescales. This island is small but apparent for all three test planet masses and in all cases the island has high FTD values, i.e., test planets in this region do not strongly perturb the orbits of planets  $b - f$ . In this island, the longitudes of pericenter of planets  $d$  and  $g$  librate with low amplitude and eccentricities of both planets also oscillate

---

<sup>1</sup>The location of the resonance is shifted slightly from its nominal value of 2.83 AU by secular effects.

with relatively low amplitudes. Thus, this island of low-amplitude apsidal libration has very high FTD values. There is another region in Fig. 7 which exhibits low-amplitude apsidal libration, with  $a > 2.88$  AU and  $e \sim 0.06$  (note that  $e_d = 0.063$ ). This region is not distinct from surrounding orbits in terms of the FTD value; nonetheless it is strongly localized. It is interesting that this libration is so strong on one side of the resonance (i.e., at orbital period ratios with planet  $d$  of less than 3:1) and nonexistent on the other side of the resonance.

Test planets near the resonant region ( $a_g = 2.86 - 2.89$  AU,  $e_g \leq 0.06$ ) or apsidal-libration island ( $a_g = 2.85 - 2.88$  AU,  $e_g = 0.15 - 0.2$ ) may undergo temporary capture into the 3g:1d resonance, i.e. temporary libration of one or more resonant arguments. However, in these cases the evolution of the system is typically chaotic such that resonant libration does not last for long times. The majority of these cases are unstable on the 10 Myr integration period, especially for smaller test planet masses  $M_g$ . For larger  $M_g$ , stable cases have small FTD values and so are observationally unlikely. In addition, we expect such cases to be unstable on longer timescales given the chaotic evolution of the system.

FTD values at large  $e_g$  are a function of  $M_g$  (see Fig. 7), as a more massive eccentric planet will impart larger perturbations on the other planets in the system. Note that these regions do not undergo resonant or apsidal libration.

We reran the same cases with the apses of planets  $g$  and  $d$  anti-aligned rather than aligned; Figure 9 summarizes the outcome. For anti-aligned apses we see the same instability of planets in the resonant region, but no island of apsidal libration was apparent. There also existed a few cases undergoing stable resonant libration of  $\theta_3$  in the same region as the aligned case ( $a_g = 2.86-2.89$  AU), but only for initial  $e_g = 0$ . The only other test planets that underwent resonant libration were for  $M_g = 90 M_\oplus$  at higher eccentricities. As before, these cases evolve chaotically and have high FTD values. Such orbits are unstable for smaller  $M_g$  and likely unstable on longer timescales for  $M_g = 90 M_\oplus$ .

The stability limits far from resonance differ between the aligned and anti-aligned simulations. In particular, the edges of the resonance occur at lower eccentricities for the anti-aligned case (at  $e_g = 0.3 - 0.35$  rather than 0.45-0.5). This appears to be due to stronger secular forcing for the cases which are initially anti-aligned. In other words, anti-aligned test planets start the simulations in a phase of eccentricity growth and aligned planets start in a phase of eccentricity decline. Thus, the long-term median eccentricity of planet  $g$  in an anti-aligned configuration with planet  $d$  is significantly larger than the eccentricity of planet  $g$  starting in an aligned configuration. Higher eccentricities lead to closer encounters with other planets, which is the key factor in determining the stability of a planetary system (e.g., Marchal & Bozis 1982; Gladman 1993; Barnes & Greenberg 2006a, 2007). Therefore, for a given starting eccentricity, a planet in an anti-aligned configuration will have a higher

average eccentricity than for an aligned configuration – this higher eccentricity will bring the anti-aligned case closer to instability. So, although the stability limit for aligned and anti-aligned cases has the same time-averaged eccentricity, this limit occurs for smaller *starting* eccentricities for the anti-aligned configuration. It is therefore important to note that the initial eccentricity is not necessarily a good measure of the typical eccentricity during an integration, especially when comparing systematically different orbital angles.

#### 4.2.2. The 4g:1d MMR

The 4:1 MMR with planet  $d$  is strongly dependent on  $M_g$  (see Figure 10). For both  $M_g = 80 M_\oplus$  and  $40 M_\oplus$ , the outskirts of the resonance at high-FTD values show the same structure. However, the heart of the resonance, at 2.35-2.36 AU, is populated with lower-FTD planets for  $M_g = 80 M_\oplus$  and is empty for  $M_g = 40 M_\oplus$ . Planets in this region undergo chaotic and temporary capture into resonant libration. However, the resonance never persists for more than a few Myr. For  $M_g = 40 M_\oplus$  we see the same phenomenon but the timescale for such planets to become dynamically unstable is shorter, such that very few survive for 10 Myr. We suspect that this chaotic region will be cleared out for  $M_g = 80 M_\oplus$  on timescales that are somewhat longer, but still short compared with the lifetime of the system. Thus, we do not expect any planets to exist in the 4g:1d MMR.

### 4.3. Neutral Resonances – 2f:1g, 3f:1g, and 5g:2d

#### 4.3.1. The 2f:1g MMR

The 2f:1g MMR is located at  $\sim 1.24$  AU. Figure 11 shows a lot of substructure within the resonance, with significant variations in FTD and stability between neighboring test planets. We believe these variations are caused by a combination of secular effects and sparse sampling. Nonetheless, we see a clear trend of higher FTD and greater stability for lower  $M_g$ .

For  $M_g > 10 M_\oplus$  only a very limited sample of test planets show evidence for libration of 2f:1g resonant angles. Indeed, for  $M_g = 30 M_\oplus$  and  $60 M_\oplus$  the only region which exhibits resonant libration is at  $a_g = 1.24$  and  $1.25$  AU, and  $e_g = 0.26$ - $0.30$ . In this region libration of  $\theta_2 = 2\lambda_g - \lambda_f - \varpi_f$  occurs but with varying amplitudes and in a chaotic fashion with occasional circulation. However, the median FTD value of these resonant planets is only 0.1 ( $M_g = 60 M_\oplus$ ) and 0.37 ( $M_g = 30 M_\oplus$ ). A large range of parameter space exhibits temporary libration of resonance angles but no long-term resonance. This region is centered

at 1.24-1.25 with somewhat smaller eccentricities, and has small FTD values. In contrast, for  $M_g = 10 M_\oplus$ , several regions exhibit stable resonant libration. Resonant orbits tend to correlate with high FTD values in the 'V'-shaped region and tend to lie at the edges at  $a_g = 1.24$  and  $1.26$  AU.

Figure 12 shows the evolution of resonant angles  $\theta_1$  and  $\theta_2$  for two simulations, both starting with  $a_g = 1.251$  AU and  $e_g = 0.282$ , but with  $M_g = 60 M_\oplus$  and  $10 M_\oplus$ . For  $M_g = 60 M_\oplus$ ,  $\theta_2$  librates about  $0^\circ$  in irregular fashion with occasional circulation, and  $\theta_1$  circulates. For  $M_g = 10 M_\oplus$  the situation is quite different:  $\theta_1$  librates steadily about  $75^\circ$  with an amplitude of  $30^\circ$ , and  $\theta_2$  librates about  $315^\circ$  with an amplitude of  $\sim 90^\circ$  but with occasional circulation.<sup>2</sup> The contrast between the two cases is remarkable and leads us to the conclusion that it is very unlikely for a planet with  $M_g \gtrsim 20 M_\oplus$  to exist in the 2f:1g MMR.

#### 4.3.2. The 3f:1g MMR

The 3f:1g MMR lies at 1.63 AU. Figure 13 shows a clear trend between lower FTD in this region and larger  $M_g$ . Thus, the 3f:1g MMR is unlikely to contain a planet more massive than  $\sim 30 M_\oplus$ . The mean [median] values of the FTD for simulations with  $a_g = 1.633$  AU are 0.49 [0.59] for  $M_g = 68 M_\oplus$ , 0.69 [0.80] for  $M_g = 30 M_\oplus$ , and 0.97 [0.98] for  $M_g = 10 M_\oplus$ .

None of the planets with  $a_g = 1.633$  AU in Fig. 13 (the central “column” of  $a_g$  values) stay in resonance for long timescales. Resonant angles librate temporarily in many cases before switching to circulation, and sometimes back to libration in irregular fashion. Despite this chaotic behavior, most of these cases appear to be stable for 10 Myr, without undergoing close approaches with planet  $f$ . Many of the simulations with  $a_g = 1.628$  and  $1.638$  AU in Fig. 13 exhibited a period of apsidal libration between planets  $f$  and  $g$ . As for the resonant cases, periods of circulation and libration were often chaotically interspersed, but the simulations were nonetheless stable and with high FTD values. For smaller  $M_g$ , there exist fewer planets which exhibit temporary resonant libration, but the region of temporary apsidal libration is expanded. For the most part, regions of low FTD correspond to chaotic zones and high FTD correspond to temporary apsidal libration.

---

<sup>2</sup>It is uncommon for resonant angles to librate about values other than  $0^\circ$  or  $180^\circ$  but can happen in some circumstances (e.g., Zhou & Sun 2003).

#### 4.3.3. The 5g:2d MMR

Figure 14 shows the stability and FTD of planet  $g$  in and near the 5:2 resonance with planet  $d$ . The structure of the phase space is quite simple in this case and can be broken into four regions. The first region, represented as high-FTD areas at  $e_g < 0.07$ , undergoes regular apsidal libration but is not in resonance. The second, smaller region also has high FTD values and is located at  $a_g \approx 3.20 - 3.225$  AU and  $e_g = 0.25 - 0.4$ . This region is wider for  $M_g = 50 M_\oplus$  than for  $95 M_\oplus$  but the characteristics are the same for the two values of  $M_g$ : this zone undergoes stable libration of all four resonant arguments, as well as apsidal libration. This region is therefore in the apsidal corotation resonance, also seen for large  $M_g$  in the 2g:1d MMR. The third region comprises the low-FTD region centered on the resonant region, at slightly smaller  $a_g$  and  $e_g$ . This chaotic region is where test planets may be temporarily captured into resonance or apsidal libration but the evolution is chaotic and the resonance is short-lived. The fourth and final region includes the high-FTD areas at the edges of our sampled zone, at  $e_g \gtrsim 0.1$ . This region does not participate in the resonance or apsidal libration.

For planet  $g$  to be located in the 5g:2d MMR, it must be localized in both  $a_g$  and  $e_g$ . It must reside at  $a_g \sim 3.21$  AU with  $e_g \sim 0.3$ ; this resonant region is wider for lower  $M_g$ . The surrounding region is unlikely to host a massive planet given the low FTD values. But for low  $e_g$ , the entire region is allowed and apsidal libration is preferred.

#### 4.4. The 3c:1b MMR

Planets  $b$  and  $c$  lie very close to the 3:1 MMR (Marcy *et al.* 2002; Ji et al 2003), but Fischer *et al.* (2008) note that the resonant arguments are circulating rather than librating. In other words, planets  $b$  and  $c$  are not in resonance. Since an additional planet  $g$  can affect the mean motions of other planets in the system, we calculated resonant angles of planets  $b$  and  $c$  for all of our stable 6-planet simulations. We find that, for our chosen configuration of known planets  $b - f$ , there are no cases in which planet  $g$  causes the resonant angles of planets  $b$  and  $c$  to librate. Thus, we conclude that the only way for planets  $b$  and  $c$  to truly be in a resonance is if our assumed orbital parameters for planets  $b - f$  are incorrect, which is certainly possible given the observational uncertainties.

## 5. Multiple Planets in the Stable Zone

Given the width of the stable zone between planets  $f$  and  $d$ , more than one additional planet could exist in the region. We ran additional simulations including multiple planets in the stable zone. For simplicity, we chose a fixed mass of  $50 M_{\oplus}$  for all additional planets. Planets were spaced such that their closest approach distances (perihelion  $q_1$  vs. aphelion  $Q_2$ ) were separated by a fixed number  $\Delta$  of mutual Hill radii  $R_H$ , where  $R_H = 0.5(a_1 + a_2)[(M_1 + M_2)/3M_{\star}]^{1/3}$  (Chambers, Wetherill & Boss (1996) and subscripts 1 and 2 refer to adjacent planets. We ran simulations with planets spaced by  $\Delta = 5 - 14.5R_H$  in increments of  $0.5 R_H$ , with five simulations for each separation with eccentricities chosen randomly to be less than 0.05, for a total of 100 simulations. The number of additional planets varied with the planet spacing, from five planets in the stable zone for  $\Delta = 5$  to two for  $\Delta = 14.5$ . No cases with five extra planets was stable, and only one case with four extra planets survived for 10 Myr and the evolution of that case was chaotic. However, roughly 40% (11/28) of cases with three additional planets survived. Typical configurations for stable simulations with three planets contained planets at 1.1-1.2 AU, 1.6-1.9 AU, and 2.5-2.9 AU. The vast majority ( $43/45 = 96\%$ ) of systems with two extra planets were stable for 10 Myr. These contained additional planets at 1.3-1.6 AU and 2.2-3.3 AU. All stable cases had very high FTD values ( $>97\%$ ).

## 6. Planets Exterior to Planet $d$

Figure 15 shows the survival time of test particles beyond planet  $d$  as a function of their semimajor axis. As expected, there is a several AU-wide region just beyond planet  $d$  in which low-mass planets are unstable. In this region particles' eccentricities are quickly excited to values that cause them to cross the orbit of planet  $d$ , resulting in close encounters and ejections. Farther out, there exists a narrow contiguous region of stability from 8.6 to 9 AU, which is roughly bounded by the 4:7 and 1:2 MMRs with planet  $d$ . This stable region is the only difference between our results and those of Rivera & Haghighipour (2007), who also mapped this outer region using test particles. The difference arises from the significant decrease in the best-fit eccentricity of planet  $d$ , from 0.244 to 0.063.

A plateau of stability starts at 9.7 AU and extends continuously to 30 AU, except for a very narrow region of instability at the 3:1 MMR with planet  $d$  at 12.3 AU. Thus, the innermost planet beyond planet  $d$  is likely to be located at 10 AU or beyond, although it could inhabit the stable zone at 8.6-9 AU.

## 7. Conclusions

We have mapped out the region in 55 Cancri where an additional planet  $g$  might exist. There is a broad region of stability between known planets  $f$  and  $d$  that could contain a  $\sim$ Saturn-mass planet (Fig. 1). Since observations rule out a very massive planet, our simulations suggest that the region could easily support two or possibly even three additional planets. In addition, one or more outer planets could be present in the system beyond about 10 AU. However, such distant planets would not be detectable for many years.

We examined eight mean motion resonances in detail (see Table 2). For two of these, 3f:1g (i.e., the 1:3 MMR between planet  $f$  and hypothetical planet  $g$ ) and 4g:1d, there was no stable region that exhibited regular libration of resonant arguments. Therefore, these resonances can not contain planets in the mass range that we explored. Given the very low FTD values, the 2f:1g MMR is unlikely to contain a resonant planet more massive than  $\sim 20 M_{\oplus}$ . Two other MMRs, 3g:1d and 5g:2d, may contain a stable, high-FTD resonant planet but the location of the MMRs is constrained to a very small region of  $(a_g, e_g)$  space which is surrounded by a chaotic region. Finally, three MMRs, 3f:2g, 2g:1d, and 3g:2d, have a stabilizing influence and may contain planets near or even across the collision line with planet  $f$  or  $d$ . Each of these MMRs contains broad regions of stable libration of resonant angles, although the locations of low-FTD libration can vary with  $M_g$ . We can therefore only weakly constrain the presence of an additional planet in one of these resonances.

The region between planets  $f$  and  $d$  contains many MMRs which display a wide range of behavior. In addition to stable and unstable resonances, the behavior of resonant arguments is also diverse. In some regions we would expect all resonant angles to librate regularly, but in others only some librate. In two instances, planet  $g$  could be in the apsidal corotation resonance (Michtchenko & Beauge 2003; Ferraz-Mello *et al.* 2003): for large  $M_g$  in the 2g:1d MMR at the  $g - d$  collision line (see Fig. 5), or in 5g:2d MMR (Fig. 14). Moreover, we also see cases of “asymmetric” libration in which the equilibrium angle is neither  $0^\circ$  or  $180^\circ$  (see Fig. 8). Even if there are no additional planets in the  $f - d$  gap, there could be an asteroid belt in which this diverse and exotic dynamical behavior is on display.

55 Cancri is a critical test of the “Packed Planetary Systems” (PPS) hypothesis, which asserts that any large contiguous stable region should contain a planet (BR04; RB05; Raymond *et al.* 2006; Barnes *et al.* 2008). To date, two planets have been discovered in the three stable zones mapped out by BR04 and RB05 (in HD 74156 and 55 Cnc). Given the width of the stable zone between planets  $f$  and  $d$ , PPS indicates that at least one, and possibly two or three, more planet(s) should exist in 55 Cancri. We look forward to further observations of the system that may find such planets, or perhaps show evidence of their absence. Our results may be used to guide observers searching for planet  $g$  and beyond.

## 8. Acknowledgments

We are indebted to Google for allowing us to run these simulations on their machines. We thank the anonymous referee for pointing out several important issues that improved the paper. S.N.R. was supported by an appointment to the NASA Postdoctoral Program at the University of Colorado Astrobiology Center, administered by Oak Ridge Associated Universities through a contract with NASA. R.B. acknowledges support from NASA's PG&G grant NNG05GH65G and NASA Terrestrial Planet Finder Foundation Science grant 811073.02.07.01.15.

## REFERENCES

- Barnes, R., Goździewski, K., & Raymond, S. N. 2008, *ApJ*, 680, L57
- Barnes, R., & Greenberg, R. 2007, *ApJ*, 665, L67
- Barnes, R., & Greenberg, R. 2006, *ApJ*, 652, L53
- Barnes, R., & Greenberg, R. 2006, *ApJ*, 647, L163
- Barnes, R., & Quinn, T. 2004, *ApJ*, 611, 494
- Barnes, R., & Raymond, S. N. 2004, *ApJ*, 617, 569
- Bean, J. L., McArthur, B. E., Benedict, G. F., & Armstrong, A. 2008, *ApJ*, 672, 1202
- Beaugé, C., & Michtchenko, T. A. 2003, *MNRAS*, 341, 760
- Butler, R. P., Marcy, G. W., Williams, E., Hauser, H., & Shirts, P. 1997, *ApJ*, 474, L115
- Chambers, J. E. 1999, *MNRAS*, 304, 793
- Chambers, J. E., Wetherill, G. W., & Boss, A. P. 1996, *Icarus*, 119, 261
- Cincotta, P. M., & Simó, C. 2000, *A&AS*, 147, 205
- Ferraz-Mello, S., Beaugé, C., & Michtchenko, T. A. 2003, *Celestial Mechanics and Dynamical Astronomy*, 87, 99
- Fischer, D. A., et al. 2008, *ApJ*, 675, 790
- Froeschlé, C., Lega, E., & Gonczi, R. 1997, *Celestial Mechanics and Dynamical Astronomy*, 67, 41
- Gladman, B. 1993, *Icarus*, 106, 247
- Ji, J., Kinoshita, H., Liu, L., & Li, G. 2003, *ApJ*, 585, L139
- Jones, B. W., Underwood, D. R., & Sleep, P. N. 2005, *ApJ*, 622, 1091
- Laskar, J. 1996, *Celestial Mechanics and Dynamical Astronomy*, 64, 115
- Lee, M. H., & Peale, S. J. 2002, *ApJ*, 567, 596
- Marcy, G. W., Butler, R. P., Fischer, D. A., Laughlin, G., Vogt, S. S., Henry, G. W., & Pourbaix, D. 2002, *ApJ*, 581, 1375

- Marzari, F., Scholl, H., & Tricarico, P. 2006, *A&A*, 453, 341
- Marzari, F., & Weidenschilling, S. J. 2002, *Icarus*, 156, 570
- McArthur, B. E., et al. 2004, *ApJ*, 614, L81
- Michtchenko, T. A., Beaugé, C., & Ferraz-Mello, S., 2008, *MNRAS*, in press
- Morbidelli, A., Tsiganis, K., Crida, A., Levison, H. F., & Gomes, R. 2007, *AJ*, 134, 1790
- Raymond, S. N., Barnes, R., Armitage, P. J., & Gorelick, N. 2008, *ApJL*, submitted.
- Raymond, S. N., & Barnes, R. 2005, *ApJ*, 619, 549
- Raymond, S. N., Barnes, R., & Kaib, N. A. 2006, *ApJ*, 644, 1223
- Rivera, E., & Haghighipour, N. 2007, *MNRAS*, 374, 599
- Sándor, Z., & Kley, W. 2006, *A&A*, 451, L31
- Sándor, Z., Süli, Á., Érdi, B., Pilat-Lohinger, E., & Dvorak, R. 2007, *MNRAS*, 375, 1495
- Šidlichovský, M., & Gerlach, E. 2008, *IAU Symposium*, 249, 479
- Snellgrove, M. D., Papaloizou, J. C. B., & Nelson, R. P. 2001, *A&A*, 374, 1092
- Valenti, J. A., & Fischer, D. A. 2005, *ApJS*, 159, 141
- Wisdom, J., & Holman, M. 1991, *AJ*, 102, 1528
- Zhou, J.-L., & Sun, Y.-S. 2003, *ApJ*, 598, 1290

Table 1. Self-Consistent Dynamical Fit of 55 Cancri (Fischer *et al.* 2008)

Planet	M sin i ( $M_J$ )	$a$ (AU)	$e$	$\pm$	$\varpi$	$T_{peri}$ (JD-2440000)
e	0.024	0.038	0.263	0.06	156.5	7578.2159
b	0.84	0.115	0.016	0.01	164.0	7572.0307
c	0.17	0.241	0.053	0.052	57.4	7547.525
f	0.14	0.785	0.0002	0.2	205.6	7488.0149
d	3.92	5.9	0.063	0.03	162.7	6862.3081

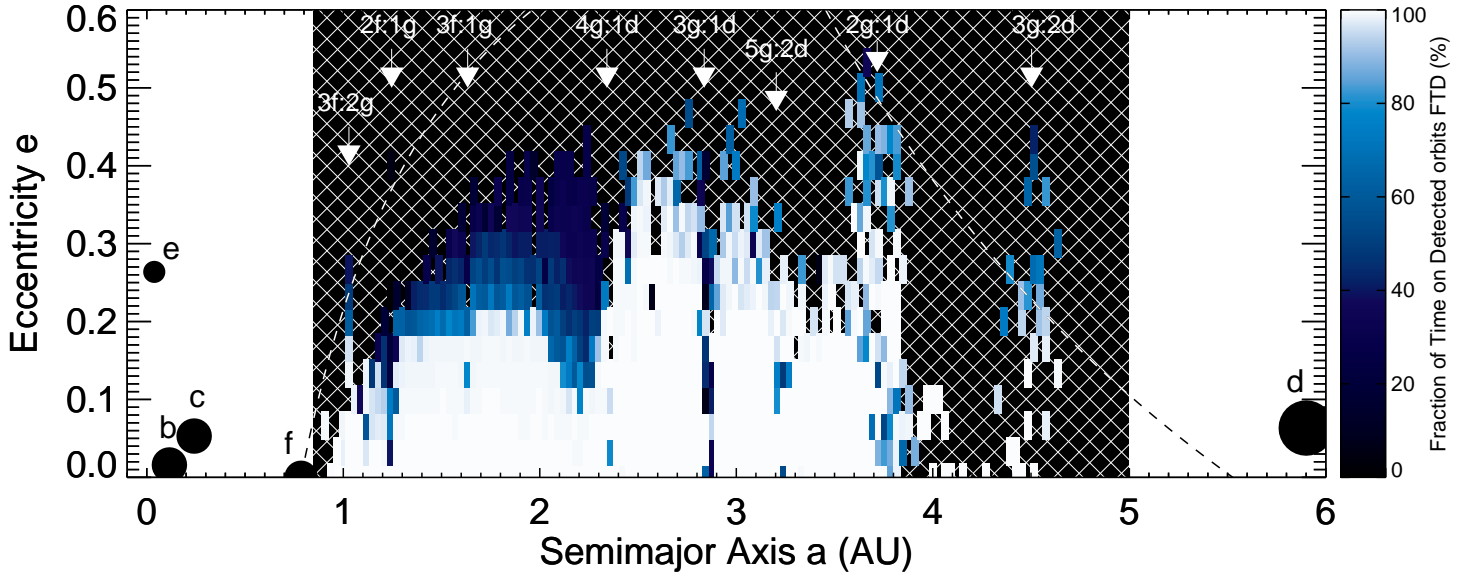


Fig. 1.— The stable zone between planets  $f$  and  $d$ . White regions represent the orbital elements of simulations with an additional test planet that were stable for 10 Myr. Black regions were unstable. Grey regions were stable but are unlikely to contain an additional planet because perturbations of the other planets’ orbits were too strong (see text for discussion). Planets  $b$  through  $f$  are labeled.

Table 2. Constraints on resonant planets

Resonance	Location (AU)	Comments
2f:3g	1.02-1.04	Resonant fingers at 1.024 and 1.034-1.039 AU. High-FTD in fingers at $e_g \lesssim 0.2$ .
1f:2g	1.23-1.26	For $M_g = 30$ or $60 M_\oplus$ resonance is limited to tiny region with very small FTD. Upper limit on resonant planet is $\sim 20 M_\oplus$ .
1f:3g	1.63	No stable planets show resonant libration.
4g:1d	2.35	No stable planets show resonant libration.
3g:1d	2.85-2.89	High-FTD resonant island exists at $a_g = 2.86 - 2.89$ AU and $e_g \leq 0.06$ . Island of apsidal libration at $a_g = 2.85 - 2.88$ AU and $e_g = 0.15 - 0.2$ .
3g:1d anti <sup>1</sup>	2.85-2.89	High-FTD resonant island exists at $a_g = 2.86 - 2.89$ AU and $e_g \leq 0.01$ . No island of apsidal libration.
5g:2d	3.20	High-FTD resonant island at $a_g = 3.20 - 3.225$ AU and $e_g = 0.25 - 0.4$ .
2g:1d	3.7-3.8	Resonant island at $a_g = 3.6 - 3.85$ AU and $e_g \lesssim 0.6$ .
3g:2d	4.4-4.6	Resonant island $a_g = 4.4 - 4.6$ AU and $e_g = 0.1 - 0.4$ .

<sup>1</sup>3:1 MMR with planet  $d$  with anti-aligned longitudes of pericenter.

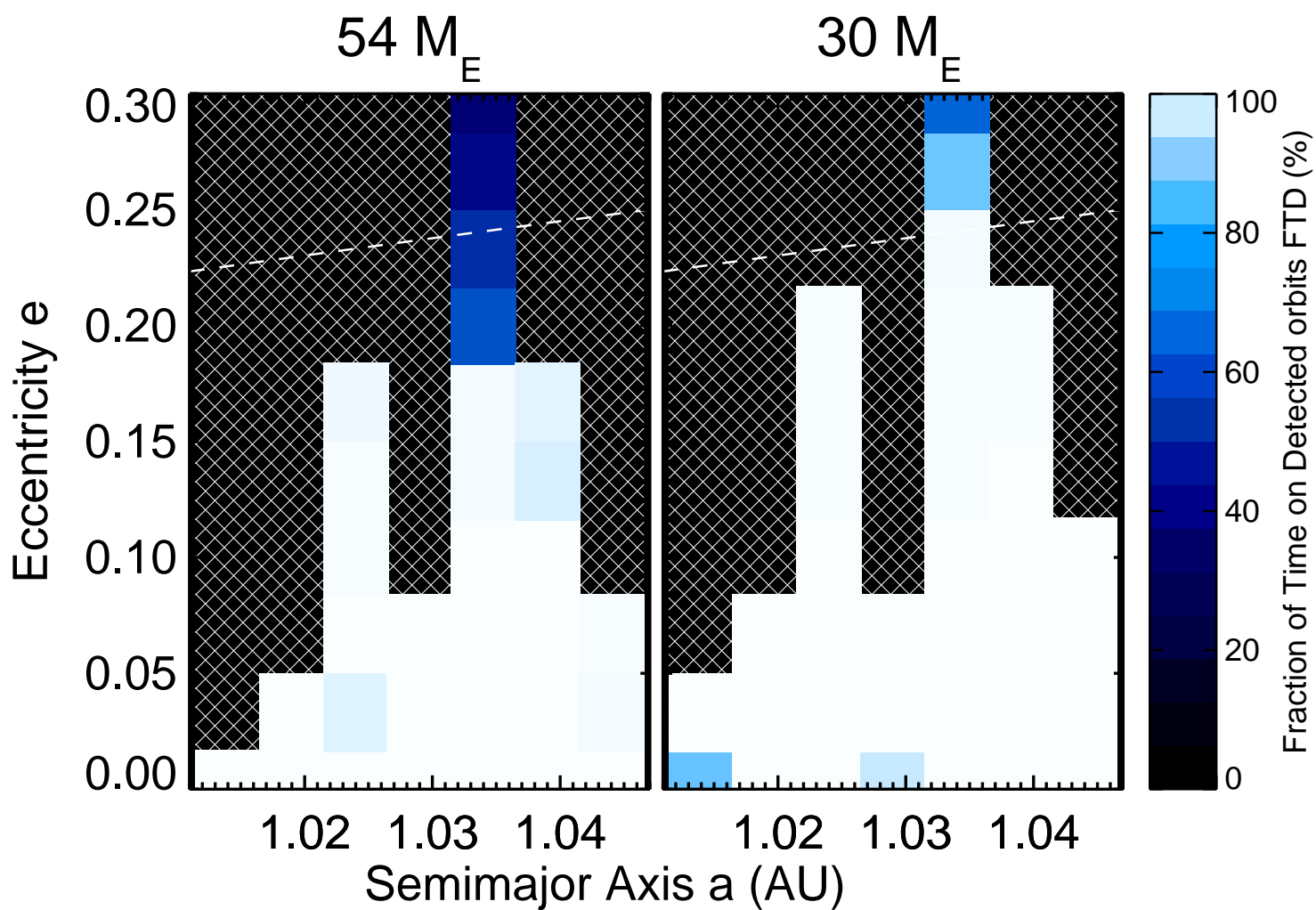


Fig. 2.— Stability and FTD of test planets in and near the 2:3 MMR with planet  $f$  (also called  $2f : 3g$ ), labeled by the test planet mass. The dashed line represents the collision line with planet  $f$ . Formatted as in Fig. 1.

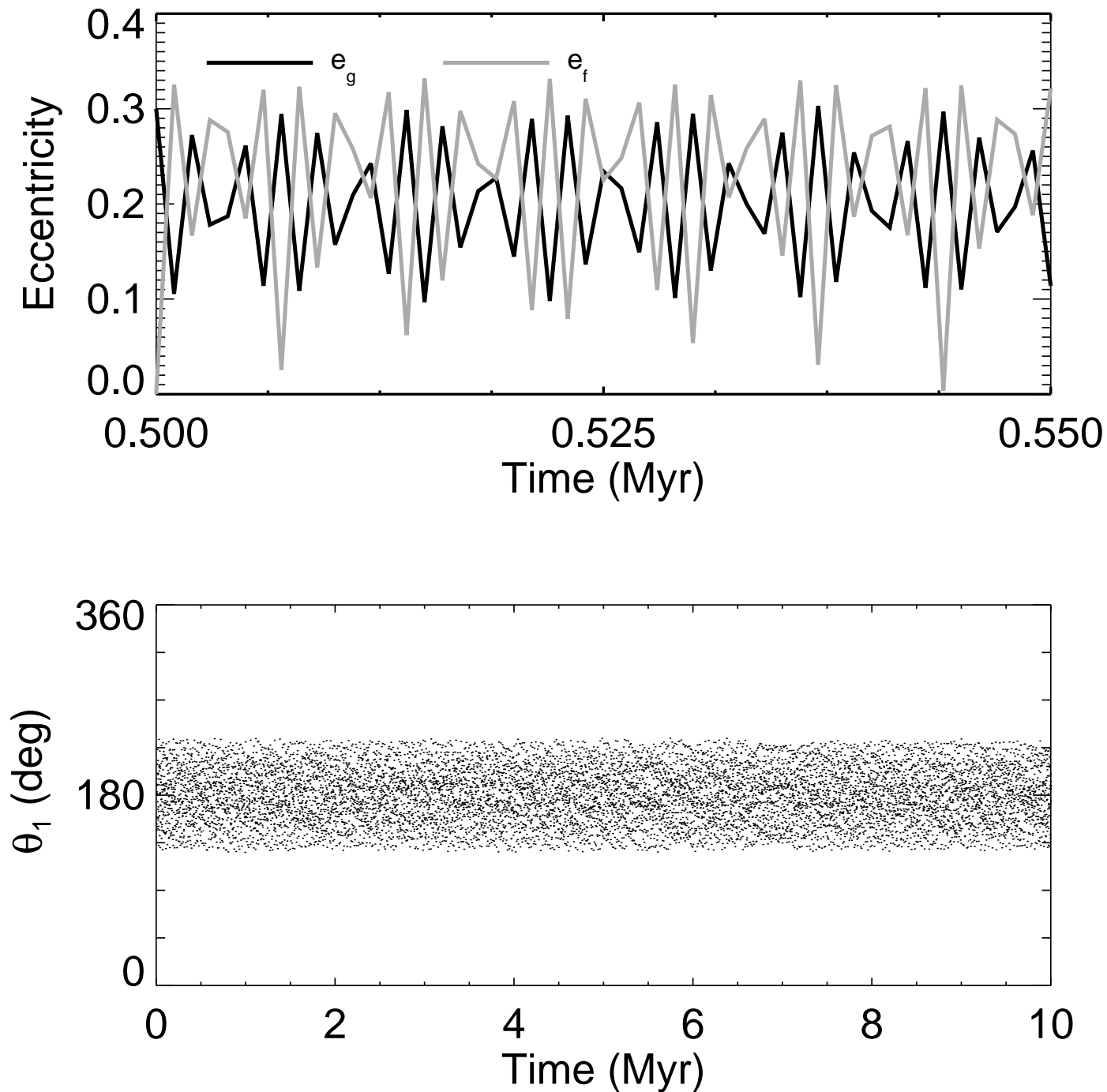


Fig. 3.— Evolution of a stable simulation in the 3f:2g MMR, with planet  $g$  starting at 1.033 AU with  $e_g = 0.3$ . **Top:** Eccentricities of planets  $g$  (black) and  $f$  (grey) for a 50,000 period of the simulation. **Bottom:** Evolution of resonant argument  $\theta_1$ .

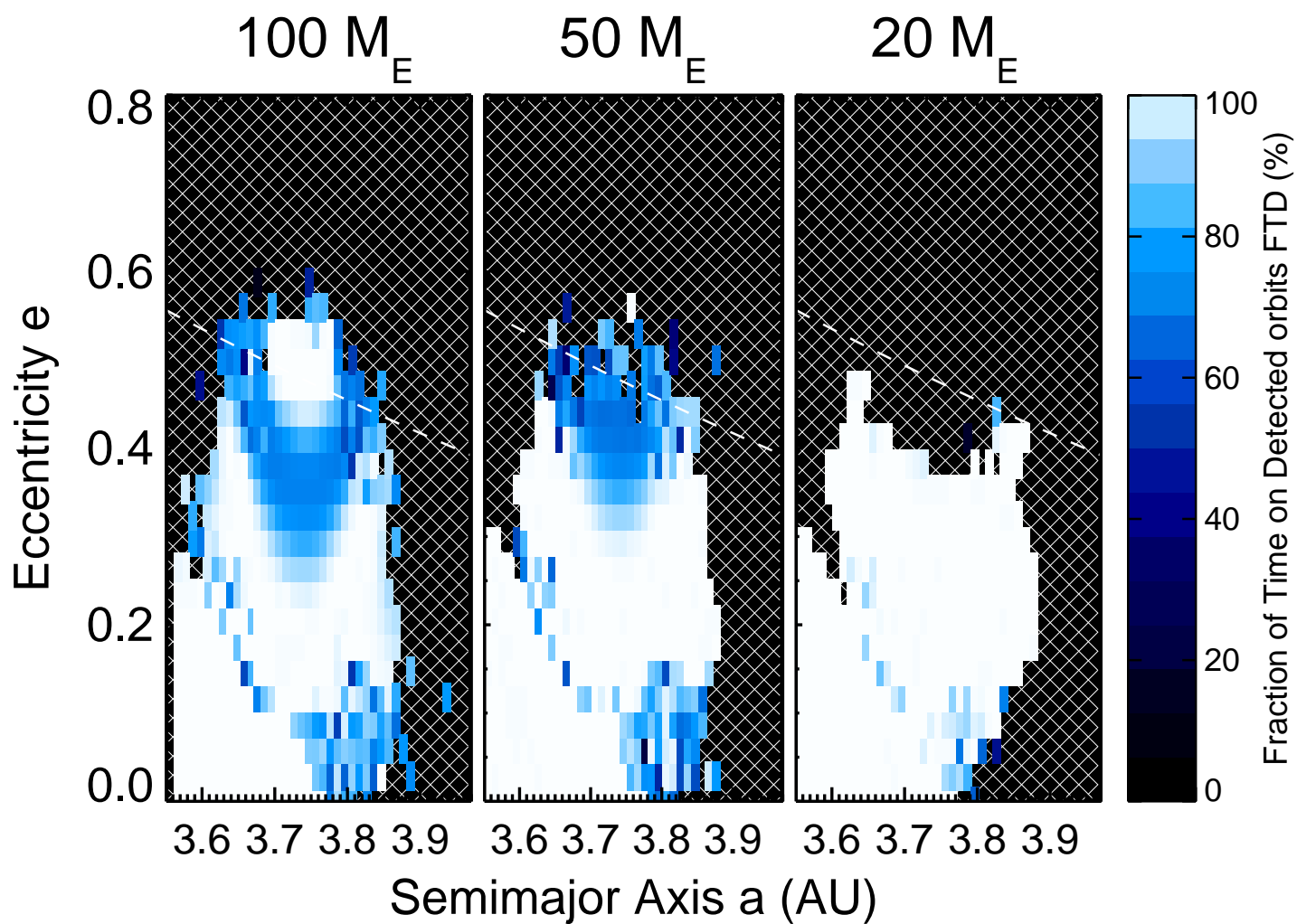


Fig. 4.— Stability and FTD of test planets in and near the 2:1 MMR with planet  $d$  (also called  $2g : 1d$ ), labeled by the test planet mass. The dashed line is the collision line with planet  $d$ . Formatted as in Fig. 1.

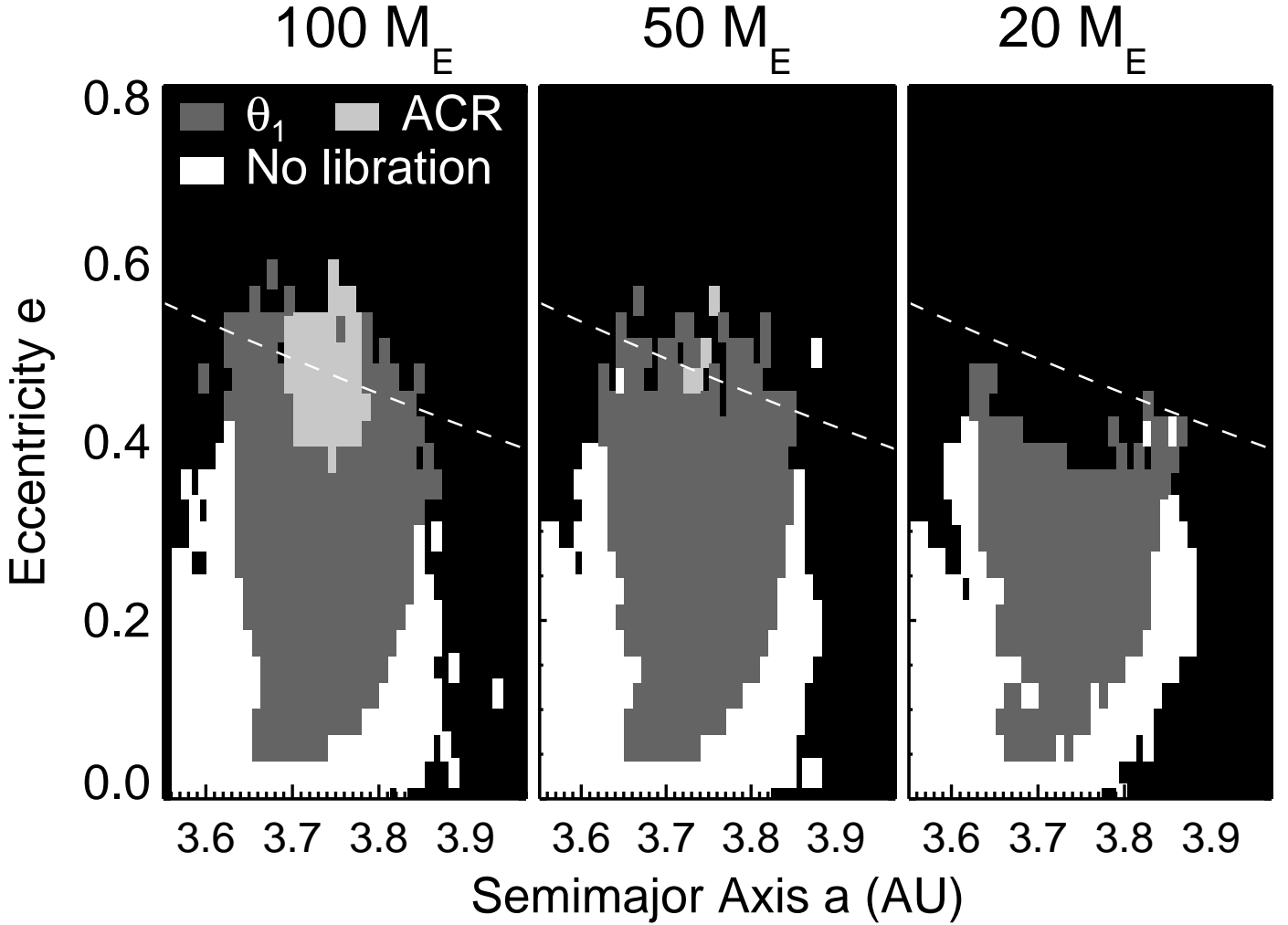


Fig. 5.— The stable zone of the  $2g : 1d$  MMR, with colors that correspond to which resonant angles are librating. White indicates no resonant libration dark grey indicates libration of  $\theta_2$  and light grey libration of  $\theta_1$ ,  $\theta_2$  and  $\varpi_g - \varpi_d$  – this configuration is called the apsidal corotation resonance (ACR). Black areas are unstable. The dashed line is the collision line with planet  $d$ .

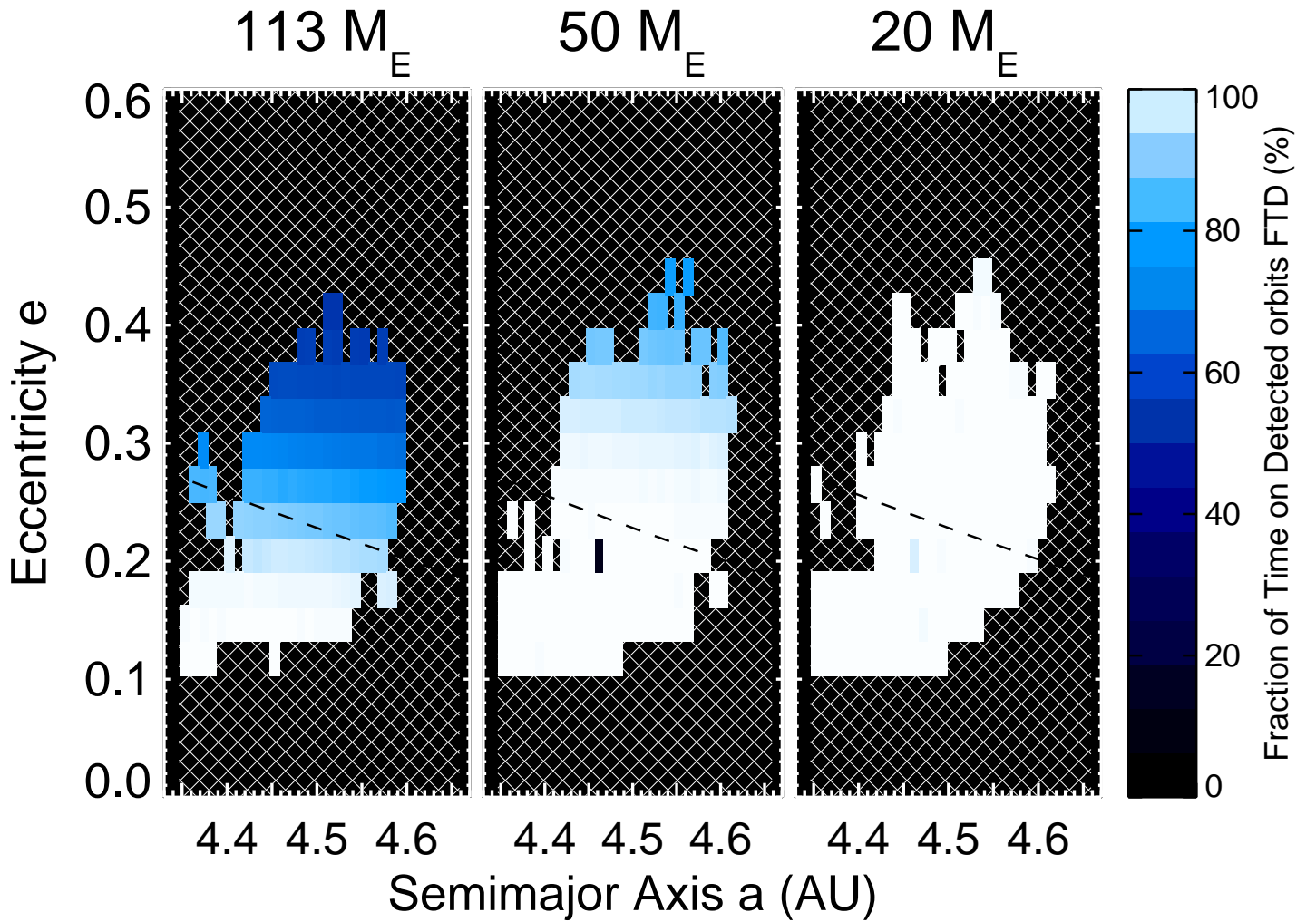


Fig. 6.— Stability and FTD of test planets in and near the 3:2 MMR with planet  $d$  (also called  $3g : 2d$ ), labeled by the test planet mass. The dashed line is the collision line with planet  $d$ . Formatted as in Fig. 1.

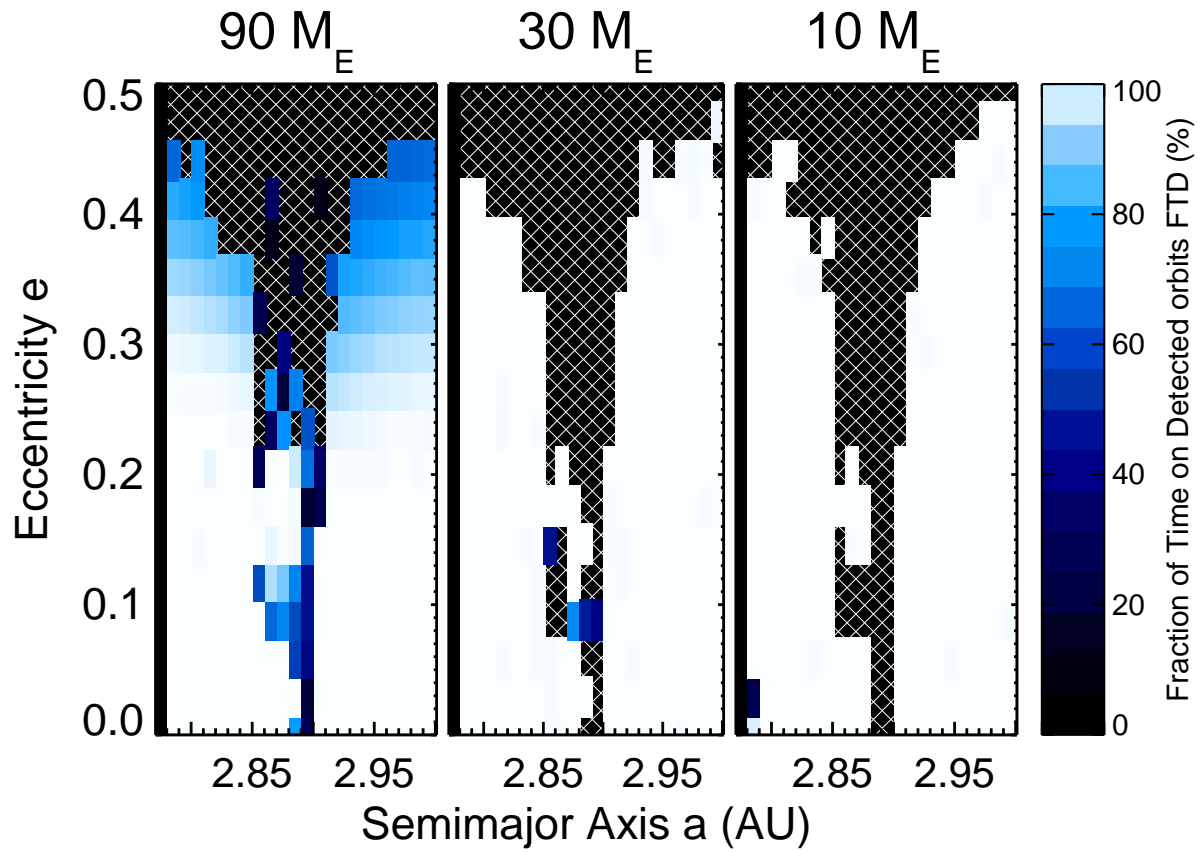


Fig. 7.— Stability and FTD of test planets in and near the 3:1 MMR with planet  $d$  (also called  $3g : 1d$ ), labeled by the test planet mass in Earth masses. Formatted as in Fig. 1.

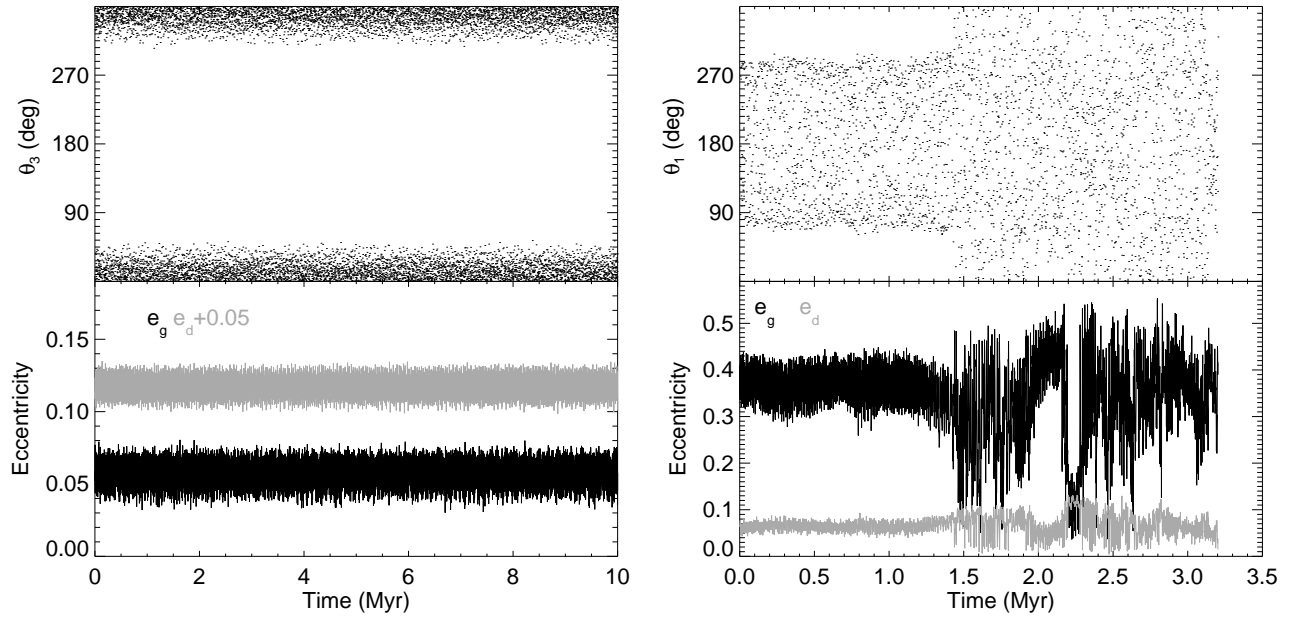


Fig. 8.— Evolution of two simulations for the 3g:1d MMR, both with  $M_g = 90 M_\oplus$ . **Left:** Evolution of  $\theta_3$  (see Eqn. 2) and eccentricities  $e_g$  and  $e_d$  for a stable resonant planet ( $e_d$  shifted up by 0.05 for clarity). **Right:** Evolution of  $\theta_1$  and  $e_g$ ,  $e_d$  for a chaotically-evolving system in the resonant region. In this case,  $\varpi_g$  and  $\varpi_d$  started in an anti-aligned configuration and librated about  $180^\circ$  for the first  $\sim 1.5$  Myr, while the system remained in resonance. This system went unstable after 3.2 Myr.

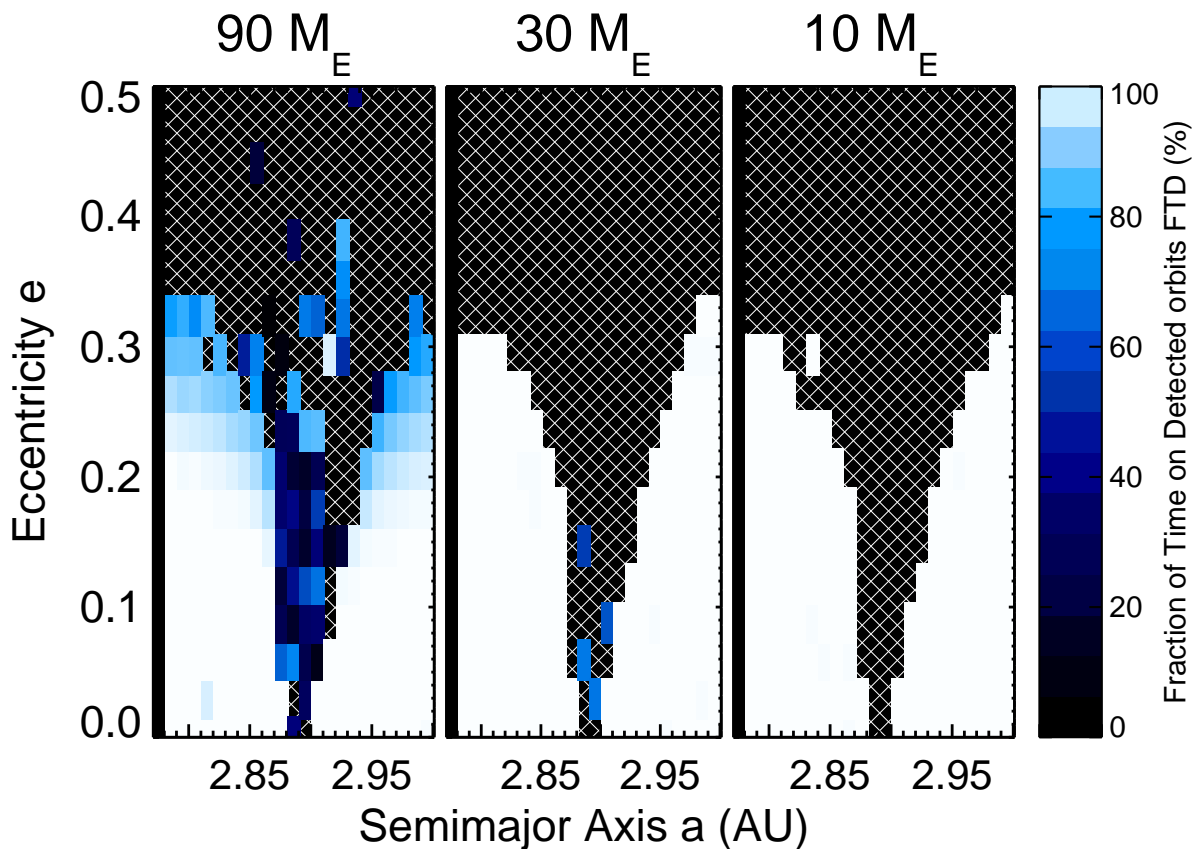


Fig. 9.— Stability and FTD of test planets in and near the 3:1 MMR with planet  $d$  (also called  $3g : 1d$ ), but with the longitudes of pericenter of planets  $g$  and  $d$  originally in anti-alignment (in Fig. 7 the apses are aligned). Again, panels are labeled by the test planet mass in Earth masses, and formatted as in Fig. 1.

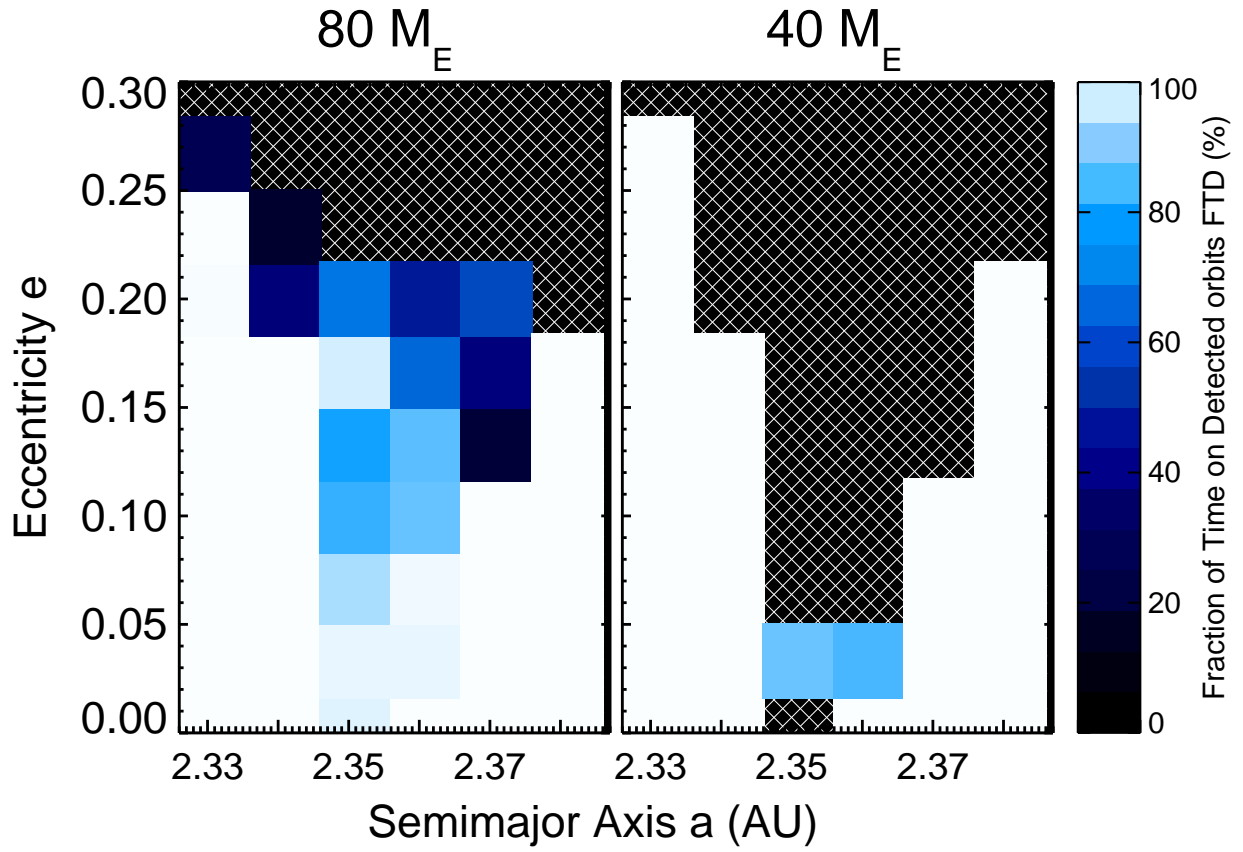


Fig. 10.— Stability and FTD of test planets in and near the 4:1 MMR with planet  $d$  (also called  $4g : 1d$ ), labeled by the test planet mass. Formatted as in Fig. 1.

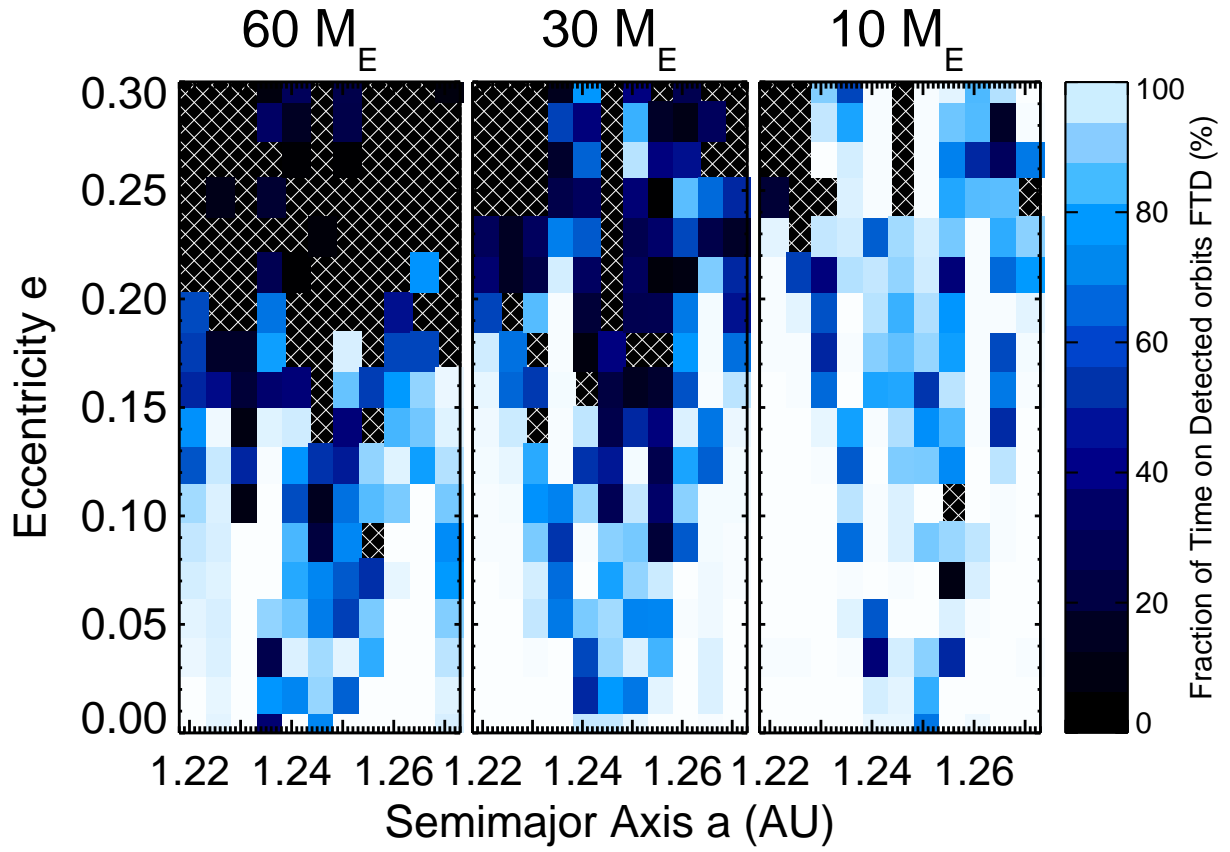


Fig. 11.— Stability and FTD of test planets in and near the 1:2 MMR with planet  $f$  (also called  $1f : 2g$ ), labeled by the test planet mass. Formatted as in Fig. 1.

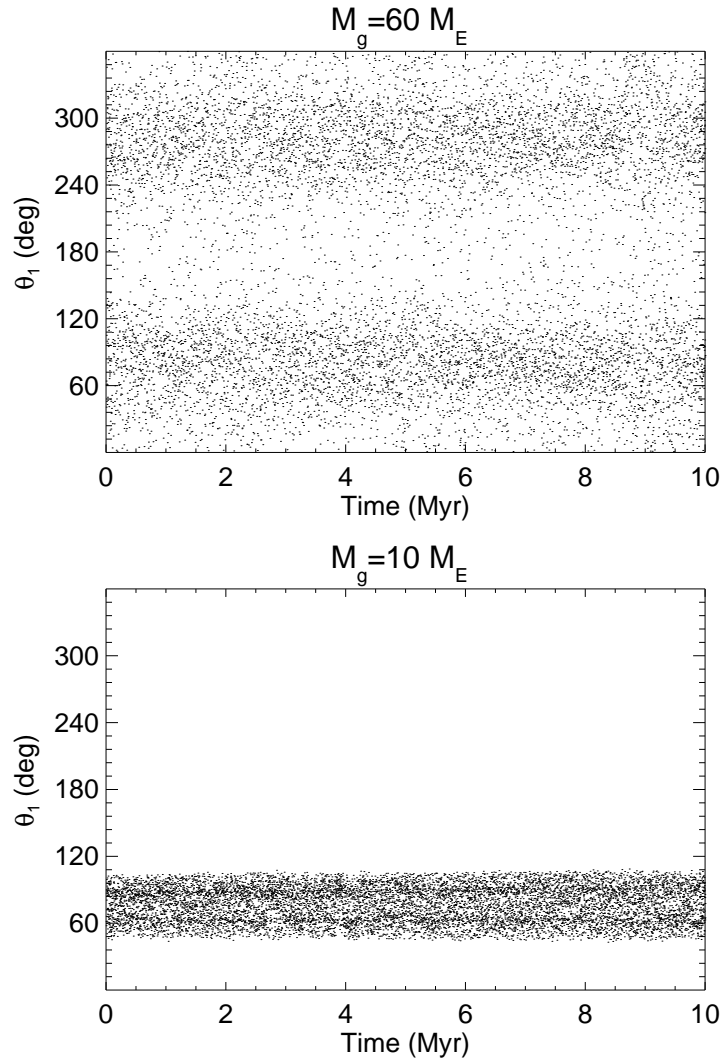


Fig. 12.— Evolution of resonant argument  $\theta_1$  for two simulations of the 2f:1g MMR. For the top panel,  $M_g = 60 M_\oplus$  and for the bottom panel  $M_g = 10 M_\oplus$ .

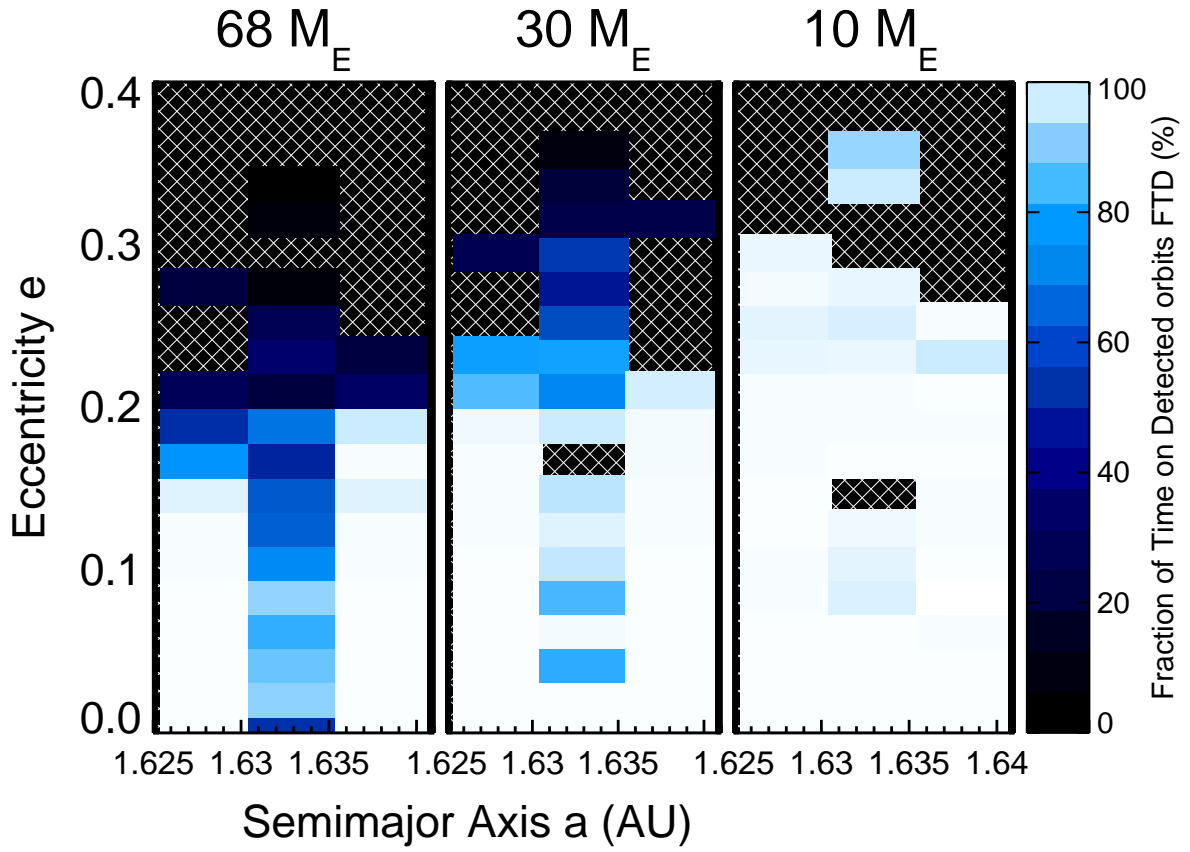


Fig. 13.— Stability and FTD of test planets in and near the 1:3 MMR with planet  $f$  (also called  $1f : 3g$ ), labeled by the test planet mass. Formatted as in Fig. 1.

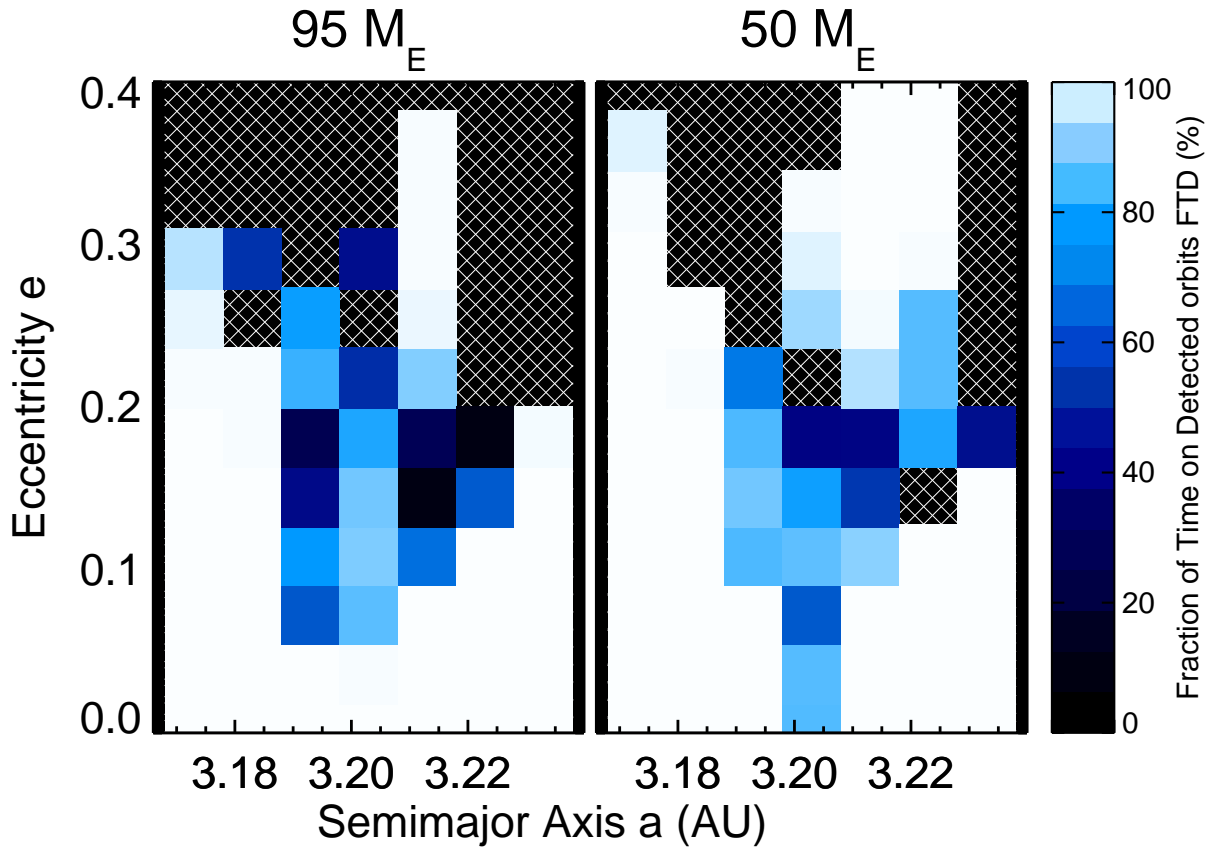


Fig. 14.— Stability and FTD of test planets in and near the 5:2 MMR with planet  $d$  (also called  $5g : 2d$ ), labeled by the test planet mass. Formatted as in Fig. 1.

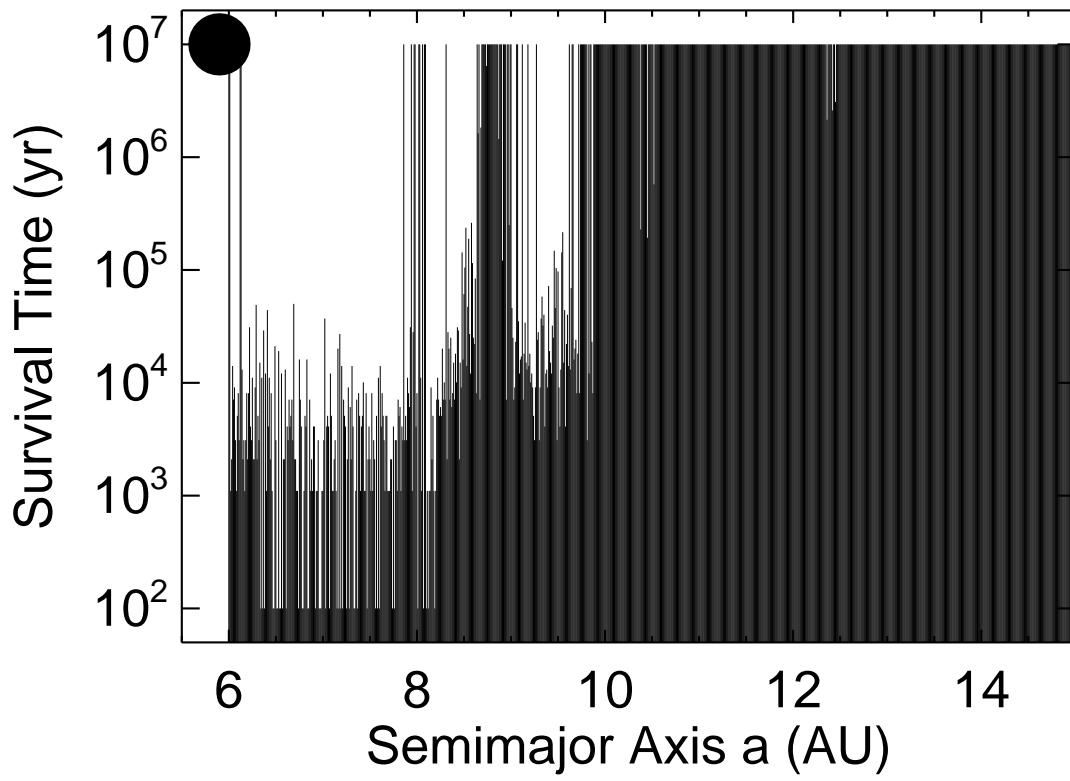


Fig. 15.— Survival time of test particles exterior to planet  $d$  at 5.9 AU (shown with black circle). Test particles extended to 30 AU; all past 15 AU were stable.